AIChE

Measurement and Interpretation of Cavitation Noise in a Hybrid Hydrodynamic Cavitating Device

Ke-Ming Quan
Corporate Engineering, Procter and Gamble Company, Cincinnati, OH 45202

Balasubrahmanyam Avvaru and Aniruddha B. Pandit
Dept. of Chemical Engineering, Institute of Chemical Technology, Matunga [E], Mumbai, India

DOI 10.1002/aic.12323
Published online July 13, 2010 in Wiley Online Library (wileyonlinelibrary.com).

In the recent past, a number of new methods of utilizing hydrodynamic cavitation to create more intense and energy efficient liquid processes have come into existence. However, it is technically challenging to characterize these processes either quantitatively or qualitatively (Patil NM, M. chemical engineering Thesis submitted to Mumbai University, India, 2001). In this work, a hybrid device producing more energy intensive cavitation has been described, which has a blade positioned in the back pressure zone (downstream side of the orifice plate). This method of cavitation production route has been quantitatively described in the form of hydrophone measured pressure signals. Fast Fourier Transform analysis (FFT) analysis has been applied to the signal obtained at various positions of the blade, and at different inlet and outlet (back) pressures. Qualitatively analysis in terms of cavity size distribution and the total number of cavitational bubbles has been conducted, using a slightly modified technique of inverse FFT reconstruction procedure originally developed by Avvaru and Pandit to model cavity size distribution. © 2010 American Institute of Chemical Engineers *AIChE J,* 57: 861–871, 2011

Keywords: cavitation, bubble size distribution, acoustic emission spectra, inverse FFT reconstruction, resonating blade

Introduction

During the past few decades, a number of technologies have been developed, each of which offers the hope of providing chemists with innovative routes of synthesis and chemical engineers with sophisticated methods of introducing the energy to bring about the desired chemical and physical change. Cavitation is one such innovative technology and has a tremendous potential to bring the chemical and physical changes from simple oxidation reaction[1] to complicated nuclear fusion reaction.[2] A measure of optimism is justified as this discipline has gained acceptance and now sustains a wide range of applications in physical and life sciences. Sono-chemistry has certainly moved a long way from its beginning in the late 1920s through its renaissance in the 1980s to where it stands as a valuable store of knowledge, especially within the community of synthetic chemists. Engineers are now succeeding in making this technology to serve for the industrial needs, to name a few, speeding up of transesterification reaction, ballast water treatment, nanoparticle synthesis, sono-crystallization, and various food (juice) emulsification processes, etc. However, a crucial hindrance in the successful application of sono-chemical reactors on an industrial scale[3] has been the lack of suitable large-scale design strategies coupled with the fact that intense cavitational activity is obtained very close to the transducers[4] (device used

Correspondence concerning this article should be addressed to A. B. Pandit at ab.pandit@ictmumbai.edu.in.

for generating ultrasound), and the existing conventional designs do not give substantial efficacy at larger scales of operation, the frequent erosion of the ultrasonic surfaces hindering the pilot plant scale operation. In spite of extensive research, there is hardly any chemical process carried out on an industrial scale owing to the lack of expertise required in diverse fields such as material science, acoustics, chemical engineering, etc., for scaling up the successful lab-scale processes.

A pilot scale multiple-frequency acoustic reactor has been used in the recent past with great success as compared with the conventional designs such as ultrasonic horn or ultrasonic bath and with substantially higher processing capacities (in the range of 10^{-3} m^3 to 1 m^3 as against few milliliters in the case of ultrasonic horn/bath). Hydrodynamic cavitation,[5] an alternative means of cavitation production, can simply be generated by the passage of the liquid through a constriction such as throttling valve, orifice plate, venturi, etc. A careful design of the system allows generating cavity collapse conditions similar to acoustic cavitation thereby enabling different applications requiring different cavitational intensities, which have previously been successfully carried out using acoustic cavitation but here with much lower energy inputs. A recently concluded classical work of Mahulkar et al.[6] has shown the energy efficiency of these reactors can be successfully increased by steam induced nucleated cavitation.

Most of the studies carried out so far in this field have restricted themselves to the study of hydrodynamic and acoustic caviation separately. Senthilkumar and Pandit[7] proved that the hydrodynamic cavitation is more energy efficient in the generation of cavities, whereas cavity collapse in acoustic cavitation was much more violent. Patil (Submitted) has shown experimentally the combination of these two cavitation techniques have the synergetic effects in the decomposition of Rhodamine-B dye solution. Hence, it would be possible to design such a system where efficient generation of the cavities took place by hydrodynamic means and then the cavities were subjected to an acoustic irradiation source wherein they are made to collapse far more violently as compared with their natural collapse hydrodynamically. Arakeri and Chakraborty[8] have proposed a technique for the hydrodynamic cavitation control and elimination that too by acoustic means. In piping systems, hydrodynamic cavitation is well known for its destructive capabilities like material damage and generation of intense noise. For these reasons, the principal aim has been to avoid or control it. Their work has suggested the use of two devices, namely, the ultrasonic nuclei modulator and the ultrasonic pressure modulator, for the prevention and control of cavities generated hydrodynamically. It has been shown that, by introducing the acoustic device upstream of the location, where the cavities are generated hydrodynamically (orifice, venturi, etc.) and the cavitation effects can be nullified. Using bubble dynamic equations (Rayleigh–Plesset equation), by appropriately changing the frequency and pressure amplitude of these devices, particular size cavities can be formed upstream of the constriction which then act as initial nuclei for hydrodynamic cavitation. These initial nuclei are responsible for the way in which the cavities behave downstream of constriction. By suitably manipulating their size, less violent collapses and in some cases no collapse (oscillatory behavior) can be achieved. The function of ultrasonic nuclei modulator is to preuse existing potential nuclei through their manipulation with ultrasonic waves, whereas the ultrasonic pressure modulator superimposes a ultrasonic field over the basic pressure field to control the maximum extent of cavity (bubble) growth, and hence, the violence of collapse (Alve V, M. chemical engineering Thesis submitted to Mumbai University, India, 2001).

Acoustic cavitation and hydrodynamic cavitation have been studied independently earlier and the effects of various operating parameters have also been studied in detail. Patil (Submitted) has experimentally shown the synergetic effects of the combination of cavitation techniques, and concluded that these synergetic effects depend on the distance between the orifice plate and the position of the ultrasonic device. Because, if the cavity enters the ultrasonic zone before its complete growth, then it may starts oscillating like a stable cavity or cavity may collapse before entering the ultrasonic zone due to the pressure recovery resulting into no synergism. For an effective utilization of hybrid cavitational effects to industrial needs, it is important to optimize the distance between the orifice plate and the ultrasonic flow cell so that the cavity enters in the ultrasonic zone immediately after its complete growth.

A liquid whistle represents a different design of the hybrid cavitation technique having a naturally resonating blade in the downstream side of the orifice plate, which serve as an acoustic source. The energy consumed for the acoustic device for the hybrid cavitation device can still be reduced by using the turbulent energy of the fast issuing stream of flow from the orifice, at the expense of small additional permanent pressure drop, where the blade acts as a frequency amplifier. The general fluid turbulence and the turbulent fluctuating frequencies cannot have frequencies in the ultrasonic/acoustic frequency range but the presence of a freely suspended blade can bring about this frequency amplification. For the industrial application of this hybrid hydrodynamic cavitation technology, particularly for the intensification of various physical processes controlled by micro mixing (interfacial surface area) of different phases involved in the process, the quantification of net cavitational effects (cavitation noise) in the form of bubble size and number distribution is required. In this work, systematic experiments have been carried out to find out the impact of the distance between the orifice and the blade, the effect of magnitude of inlet pressure and the back pressure on the net hybrid cavitation (cavitation noise). The hydrophone signals have been quantified in terms of frequency spectrum. The size and population of the cavities have been modeled using the inverse FFT reconstruction technique originally developed by Avvaru and Pandit.[9]

The entire theme of measurement of cavitational bubble size is based on the Minnaert's equation, which is originally developed by Minnaert[10] in 1933. The measurement of cavitation bubble density is based on the scheme proposed by Pandit et al.[11] A combined mathematical model has been derived earlier for the application of these two equations to the field of acoustic cavitation bubbles by Avvaru and Pandit,[9] and they have successfully determined the cavitation bubble size in the range of 60–80 μm for the ultrasound irradiation frequency of 20 kHz. Unlike the acoustic cavitation bubbles, hydrodynamic

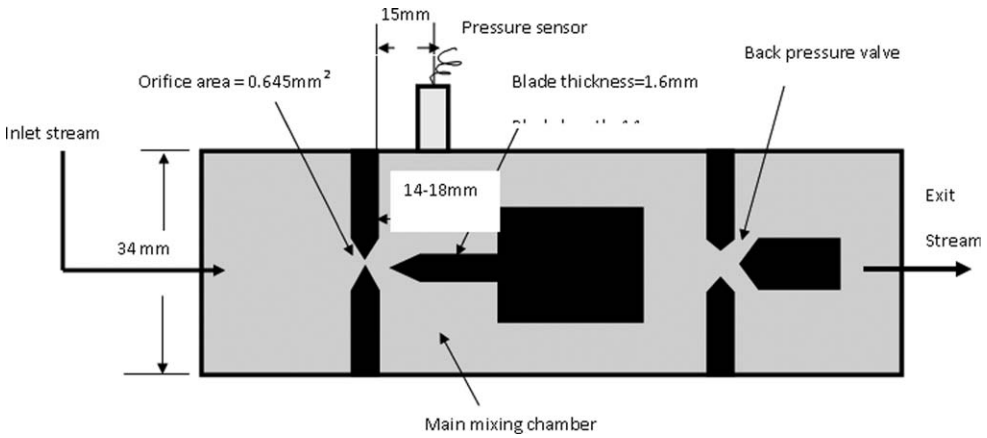

Figure 1. Schematic diagram of the experimental setup.

cavitational bubbles behave differently. These bubbles are driven by interference of fluid kinetic energy (i.e., fluid pressure) along with the turbulent fluctuating velocity, which is similar to the work of Pandit et al.,[11] i.e., measurement of bubble size in a stirred tank using acoustic emission spectra. This work of measurement of bubble size distribution and its number density in hybrid hydrodynamic cavitation under various parameters is the extension of the above two classical works under different cavitating conditions.

Theory of Cavitation Noise

Cavitation is defined by Knapp[12] as the condition when a liquid reaches a state at which vapor cavities are formed and grow due to static-pressure reductions below the vapor pressure of the liquid at constant temperature. In a flowing liquid, the likelihood of the onset of cavitation is described by the dimensionless cavitation inception number defined as

$$C = \frac{P_b - P_v}{\frac{1}{2}\rho V^2} \tag{1}$$

Where P_b is the static pressure in the main mixing chamber shown in the Figure 1, P_v is the vapor pressure of the liquid at the operating temperature, ρ and V are the liquid density and the velocity, respectively. These cavities are subjected to a pressure recovery in the flow away from the orifice. The pressure increase stops and reverses the cavity growth, resulting into implosive collapse.

Cavitation noise

The violent and catastrophic collapse of cavitational bubbles results in the production of noise. The spectrum of noise produced by a cavity during its collapse is closely related to its size. Large cavities generate low-frequency noise, whereas small cavities generate high-frequency noise. This can be seen from Eq. 2 that the collapse time for big cavity is longer than that of small ones. Assuming that the bubble collapses from a maximum radius of R_o to a minimum (critical) radius of R_c, the collapse time "τ" may be approximated by the Rayleigh time,

$$\tau = 0.915 R_o \sqrt{\frac{\rho}{P_\infty - P_v}} \tag{2}$$

The cavity may rebound back a number of cycles. As it takes about the same time to rebound to the next maximum radius, the oscillating frequency of a cavity as it collapses and rebounds can be obtained by rewriting Eq. 2 Yan et al.,[13] as

$$f_o = \frac{1}{2}\,\frac{1}{0.915 R_o}\sqrt{\frac{P_\infty - P_v}{\rho}}. \tag{3}$$

The factor [1/2] refers to rebound, which takes about the same time to reach the next maximum radius. It is important to point out that as energy dissipates into heat and sound, the rebound radius is reduced after each collapse, and therefore, the oscillating frequency changes over the whole period of oscillation. Furthermore, the growth of the cavity depends on the age history of its trajectory in the turbulent flow field. A distribution of the cavity size is, therefore, expected at any given time. All of these variations are expected to contribute to the spectrum of cavitation noise. Based on these factors, a cavity size distribution has been determined using a Minnaert's equation originally proposed by Minnaert[10] and in the recent past successfully used for the measurement of bubble size distribution of the acoustic cavitational bubbles by Avvaru and Pandit,[9]

$$f_o = \frac{1}{2\pi}\left(\frac{3\gamma P_\infty}{\rho R_o^2}\right)^{1/2} \tag{4}$$

Avvaru and Pandit[9] have developed a simplified expression for pressure radiated by the oscillating bubble at a distance of "r" from its center, with certain valid assumptions, and the total number of oscillating bubbles of frequency "f_o" in a sphere of influence of radius "r" is given by Eqs. 17 and 18 of Avvaru and Pandit,[9] and these equations rewritten as following,

$$p_r = \frac{(3\gamma P \rho)^{1/2}}{\pi f_o r} \tag{5}$$

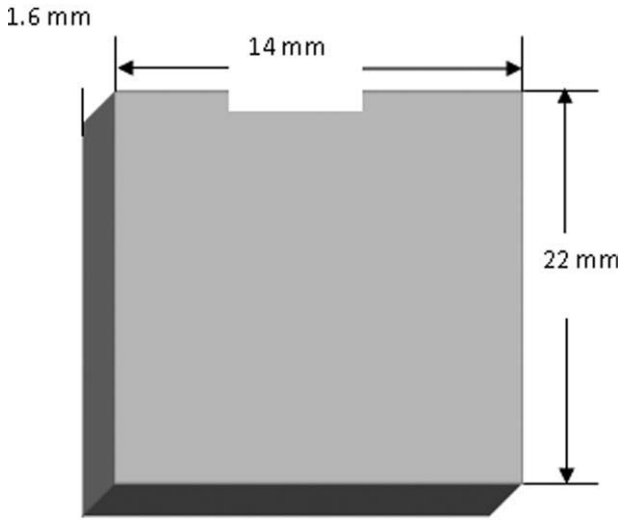

Figure 2. Resonating blade configuration.

$$n = \frac{P_{\text{res}}^2}{(3\gamma P\rho)}(\pi f_o r)^2. \tag{6}$$

Vibrations of the blade

The resonating blade arrangement and the details have been shown in Figure 2, where one end of the rectangular plate is clamped to the blade holder, and the other three sides are free. Assuming that the plate has a length of "a" (from the clamping position), width of "b" and thickness of "h". The natural frequency of this blade arrangement can be expressed by Blevins,[14]

$$f_{ij} = \frac{k_{ij}^2}{2\pi a^2}\left[\frac{\lambda h^2}{12\rho(1-\upsilon^2)}\right]^{1/2} \tag{7}$$

where f_{ij} is the resonant frequency at mode indices (i, j), i being the mode number in length, j being the mode number in width, k_{ij} is a dimensionless frequency parameter, λ is the modulus of elasticity, ρ is the density, and υ is Poisson's ratio.

The longitudinal wave velocity C can be expressed as

$$C = \sqrt{\frac{\lambda}{\rho}} \tag{8}$$

Substituting Eq. 8 in Eq. 7, it becomes,

$$f_{ij} = \frac{k_{ij}^2}{2\pi a^2} Ch\left[\frac{1}{12(1-\upsilon^2)}\right]^{1/2} \tag{9}$$

Experimental Methodology

Cavitation can be generated through different mechanisms. Hydrodynamic cavitation reactors are shown to be orders of magnitude more energy efficient than ultrasonic reactors, high-shear mills, or high-pressure homogenizers.[15] The equipment used in the this study is a Sonolator, manufactured by Sonic Corporation (Stradford, CT). It is a commercial liquid processor that utilizes hydrodynamic cavitation energy. The system is schematically illustrated in Figure 1, and it is essentially an orifice reactor, where the jet of liquid flow from the orifice is directed at a knife blade. The blade, which is clamped from behind by the blade holder, is expected to vibrate at its resonant frequency upon impingement of the jet. The vibration of the blade is believed to further enhance the cavitation noise. The operating variables of the resonating blade include inlet pressure, back pressure, and the distance gap between the blade tip and orifice. All of these operating variables are expected to have an impact on cavitation occurring within the cavitating chamber, which may in turn impact the liquid process. Sonic provides an acoustic meter that integrates the total acoustic output from the Sonolator and has recommend the users to maintain a certain level of the acoustic output by adjusting the operating parameters.

The cavitation noise was measured by a pressure transducer (PCB Piezotronics, Model-111A21), mounted at the same location as the acoustic sensor (after it was removed) at the top of the main mixing chamber and in direct contact with the liquid. The pressure transducer measures the dynamic pressure only and has a rise time ≤ 2 μs and sensitivity of 5.8 mV/kPa, the latter of which is used to convert the measured root-mean-square voltage into pressure reading in kPa. The signal is acquired and analyzed using Quattro DSP centric signal processing hardware (DATA Physics), which has two 24-bit Inputs, one 24-bit Output, and 94 kHz analysis bandwidth. Discrete data of the time domain signal has been captured, and it is converted into frequency spectra (FFT) using Auto-Signal 1.7, (SYSTAT), a commercial signal processing software. Tap water at room temperature as the liquid medium is used in this study. The orifice used in this study is supplied by Sonic Corporation, which takes a cat eye shape and has cross sectional area of 0.645 mm^2.

To confirm experimentally, the resonant frequency of the blade, the assembly of the blade, and the blade holder are taken out of the Sonolator to have the pressure sensor directly mounted onto the surface of the blade. The primary resonant frequency of the blade is confirmed to be 4.5 kHz.

The inlet pressure, the back pressure, and the position of the blade can be adjusted independently. The inlet pressure converts into the kinetic energy (higher velocity) of the liquid jet at the orifice. As can be seen from Eq. 1, the higher the inlet pressure and smaller the cavitation number, more cavitation is expected. Increase in the back pressure increases the cavitation number, which should decrease the number density of cavitation cavities and its growth. The impact of the blade position on cavitation is expected to be more complex. When the blade is close to the orifice, its moves the high-pressure zone close to the orifice and forces the cavities to collapse prematurely. On the other hand, the fragment of the collapsed cavitation, or nuclei, will experience intense vortex shedding on either side of the blade as the jet is split and moves past the front of the blade. The nuclei should regrow and generate secondary cavitation collapsing zones on either side of the blade. When the blade position is far from the orifice, the cavitation bubbles have time to grow to larger size before they collapse. However, as the blade is now farther from the high-speed jet, the vortex shedding as the jet flows past the front edge will become less vigorous. As a result, the secondary cavitation zone will become less significant and most of the cavitation will grow

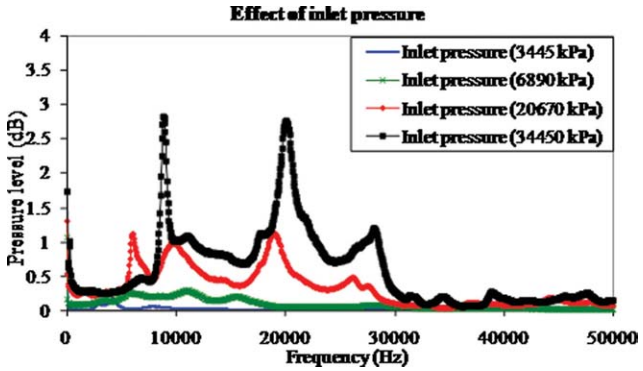

Figure 3. FFT spectrum showing the effect of inlet pressure on cavitation.

[Color figure can be viewed in the online issue, which is available at wileyonlinelibrary.com.]

and collapse before the blade. The blade may impact cavitation further if it indeed vibrates intensely in the presence of jet provided the jet has sufficient velocity/pressure to overcome blade inertia. The impact of these operating parameters on cavitation noise is the focus of this study. By preliminary examination of the FFTs obtained from the pressure signal measured by the hydrophone in the present work suggesting the response obtained is similar to our results shown in case of the acoustic cavitation system, reported in earlier work of Avvaru and Pandit.[9] Hence, it has been treated likewise to get the information necessary for the cavitational quantification in terms of bubble size and number density. The bubble sizes mentioned in this analysis are measured in terms of number mean diameter. That is, $d_{(\mathrm{avg})} = \sum n_i di / \sum n_i$.

Results and Discussion

Effect of inlet pressure

For a given orifice cross sectional area, the inlet pressure is controlled by the flow rate supplied to the cavitation device and it is measured by a pressure gauge installed at the inlet chamber shown in Figure 1. In this study, the inlet pressure (P_i) is varied in the range of 3445–34,450 kPa and its impact on cavitation noise is shown in terms of FFT spectra in Figure 3. As it can be observed from Figure 3, similarities exist in the overall distribution of the spectra at different inlet pressures. Harmonic frequencies (peaks) present at each regular interval, but the magnitude of these harmonics increasing with the increase in the inlet pressure. As the inlet pressure is increasing from 3445 to 34,450 kPa, there is an increase in the magnitude of these peaks of frequencies at higher frequency range (zone). The magnitude of these peaks has been more pronounced beyond 20 kHz frequency at higher inlet pressure conditions. This observation may be due to the prevailing of transient cavitation conditions, and hence, these frequency ranges are considered as transient collapsing cavitation bubbles. The collapse pressures have been determined using maximum mean size (calculated from the Minnaert's Eq. 4) and with the expression in Eq. 10. As the hydrophone is not in the vicinity of a collapsing cavity, instead it measures the propagated shock waves produced upon collapse of these bubbles as well as the acoustic emission of oscillating bubbles, a pressure

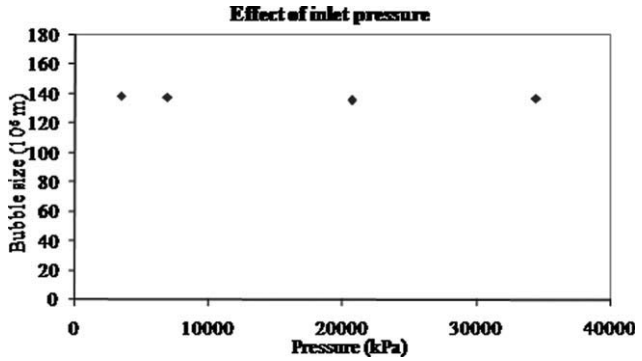

Figure 4. Effect of inlet pressure on cavitational bubble size.

dampening factor of 0.001 has been taken in the analysis (somewhat arbitrarily). That is, out of 1000 Pa, only 1 Pa is observed by the hydrophone (pressure sensor).

$$P_{\mathrm{collapse}} = P_{\mathrm{o}} \left(\frac{R_{\mathrm{o}}}{R_{\mathrm{c}}} \right)^{\gamma} \tag{10}$$

P_{v} is vapor pressure = 3200 Pa, R_{c} is critical radius assumed as 10 μm, γ is specific heat ratio of bubble content = 1.6, and R_{o} is size of cavitational bubble measured from the Minnaert's equation.

At these operating conditions, bubble size and number density of the cavitational bubbles have been modeled by the technique of Avvaru and Pandit[9] with the aforementioned modification. The modeled results are shown in Figures 4 and 5, respectively. Although the averaged bubble sizes calculated values are showing a small or no dependence of the inlet pressure, the number density (total number) of the bubbles is increasing from 11 to 6401. Note that there is uncertainty about the absolute number of the bubbles, given the arbitrary dampening factor. However, the overall number of cavitational bubbles increases with an increase of inlet pressure as shown in Figure 5. The bubble size distributions at these four operating inlet pressure conditions are shown in Figure 6, showing the increase of relatively bigger size cavitational bubbles at higher inlet pressure conditions, but the average bubble size remains nearly constant in a range of 136–140 μm. This observation indicates higher cavitation (low cavitation number) intensity at higher inlet pressure conditions.

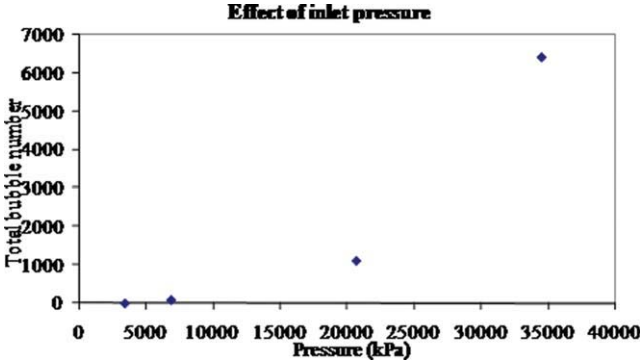

Figure 5. Effect of inlet pressure on total number of bubbles.

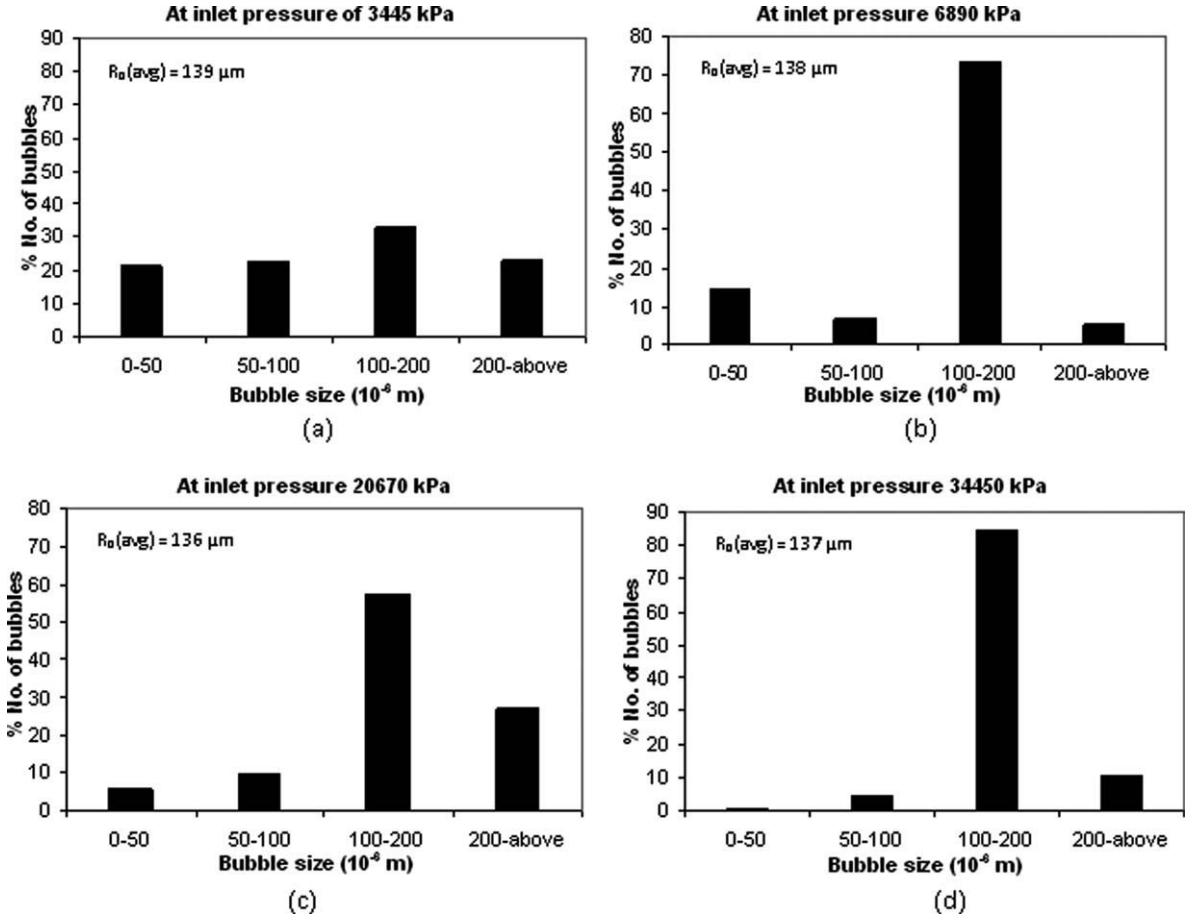

Figure 6. Effect of inlet pressure on cavitational bubble size distribution.

Impact of the back pressure

At a given inlet pressure, the back pressure can be adjusted through the back pressure valve. Typically, the extent of the back pressure adjustment is less than 10% of the inlet pressure. The impact of the back pressure on the likelihood of cavitation generation can be seen from Eq. 1. The higher is the back pressure, the higher will be the cavitation number. Therefore, the number density of cavitational bubbles will be reduced at higher back pressures. At the same time, each cavitational event is expected to collapse more intensely giving higher intensity pressure pulses. This is because the energy released during collapse of a bubble is related to the back pressure as,

$$E = \frac{4}{3}\pi R_o^3 P_\infty \tag{11}$$

Where P_∞ is the pressure away from the cavity, and can be approximated to the back pressure.

The averaged power from the collapsing cavitation can, therefore, be expressed as

$$W = \dot{E} = \frac{4}{3}\pi R_o^3 \frac{P_\infty}{\tau} \tag{12}$$

Substituting τ from Eq. 2, the intensity of cavitation is related to the back pressure by the following expression,

$$W = \frac{4}{3}\pi R_o^3 \frac{P_\infty}{\tau} \approx 4.58 R_o^2 \sqrt{\frac{P_\infty^3}{\rho}} \tag{13}$$

This suggests that the individual cavitational bubble has a tendency to collapse more intensely under a higher back pressure.

Figure 7 is the FFT spectrum showing the effect of back pressure on cavitation at a constant inlet pressure of 6890 kPa. In contrast to the lower back pressure, the spectrum at 144.69 kPa back pressure (higher back pressure) shows a reduced amplitude at low-acoustic frequencies but an increased amplitude at higher acoustic frequencies. The high-acoustic output at the higher back pressure is consistent with more intense collapse of individual cavitation. Separately, the shift of the spectra to higher frequencies implies that the mean cavitation bubble size is reduced at increased back pressure. Similarly, Figure 8 shows the effect of back pressure at a constant inlet pressure of 20,670 kPa. Again, the effect of increased back pressure is showing as a reduction in the pressure amplitude at the low acoustic frequencies but an increase at high frequencies.

Figure 9 is the modeled cavitation bubble size at these operating conditions, showing the average bubble size is decreasing from 167 to 138 μm (total number of calculated bubbles are increasing from 14 to 99) as the back pressure is increasing from 68.9 to 144.7 kPa at constant inlet pressure

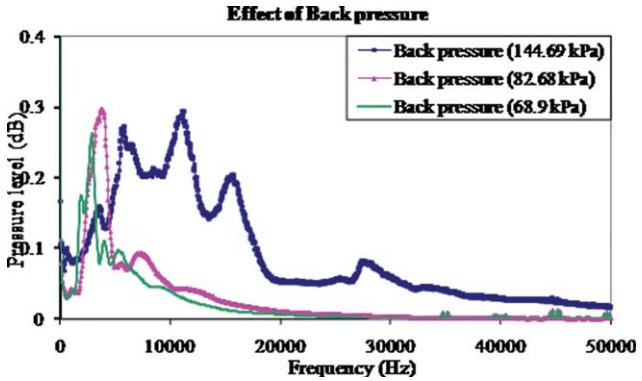

Figure 7. FFT spectrum showing the effect of back pressure at 6890 kPa inlet pressure.

[Color figure can be viewed in the online issue, which is available at wileyonlinelibrary.com.]

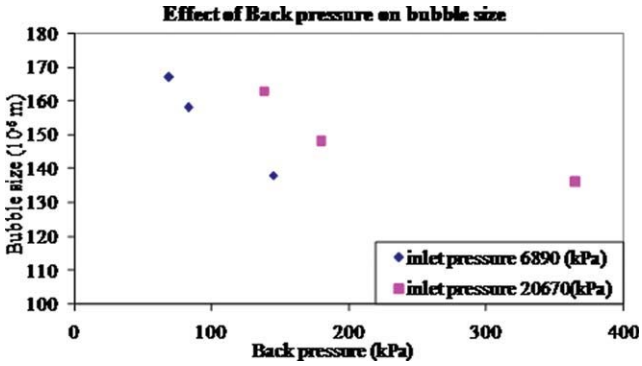

Figure 9. Effect of back pressure on cavitational bubble size.

[Color figure can be viewed in the online issue, which is available at wileyonlinelibrary.com.]

of 6890 kPa. Similarly, the average bubble size is decreasing from 163 to 136 μm (total number of calculated bubbles are increasing from 546 to 1117) as the back pressure is increasing from 137.8 to 365.17 kPa at a constant inlet pressure of 20,670 kPa. The total number of calculated bubbles is increasing with an increase of back pressure, and this increasing trend is shown in Figure 10. However, Figures 11 a, b are the photographs of the cavitation cloud with in the Sonolator, showing the reverse trend. The shaded areas reflect are the volume of bubbles occurring at the operating conditions of high-back pressure and low-back pressure conditions, respectively. It is clear from these photographs that the magnitude of the bubble density at high-back pressure conditions is lower than the low-back pressure conditions. This observation is contrary to the total number of calculated bubbles. A possible reason for this discrepancy may be the dampening factor (0.001) chosen for this analysis, which is taken on an arbitrary basis. The real situation of this dampening factor seems to vary with the bubble size and bubble fraction (higher vapor holdup) is increasing dampening factor. The magnitude of the pressure pulse produced from a single large bubble under high back pressure conditions seems to produce higher collapse pressure compared to relatively smaller bubbles. Different size bubbles located at different distances from the sensor produce differently damped responses showing different bubble size distributions and volume fraction occupation as a function of sensor location and back pressure conditions.

Figures 12 and 13 show the bubble size distributions at these operating conditions. Showing the peak of the bubble size distribution shifting toward the smaller size as the back pressure is increasing.

Effect of blade position

Figure 14 is the FFT spectrum showing the comparison of the acoustic noise in the presence of the blade when located at various distances from the orifice and also in the absence of the blade at the inlet pressure of 3445 kPa and back pressure of 62 kPa. As the blade is moving away from the orifice from a distance 2.2 to 8.8 mm, the peak amplitude of the acoustic noise shifts to the lower frequency range accompanied with a reduced amplitude. It shows that the interaction of the fast issuing jet of flow on the resonating blade becoming less intense, and hence, its effect on the hydrodynamic cavitation is decreasing. The FFT spectra with and without the blade are the same when the blade is at 8.8 mm away from the orifice, indicating no effect of the blade beyond the distance of 8.8 mm from the orifice. The calculated bubble

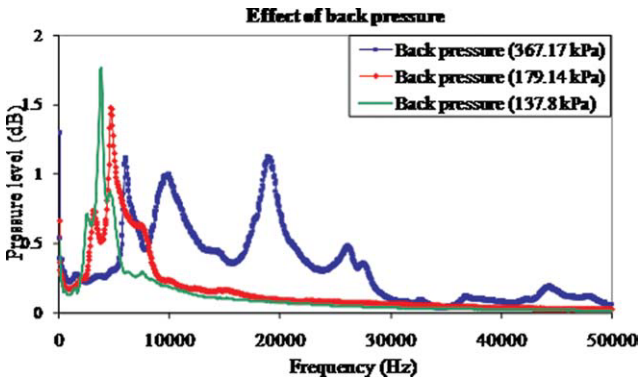

Figure 8. FFT spectrum showing the effect of back pressure at 20,670 kPa inlet pressure.

[Color figure can be viewed in the online issue, which is available at wileyonlinelibrary.com.]

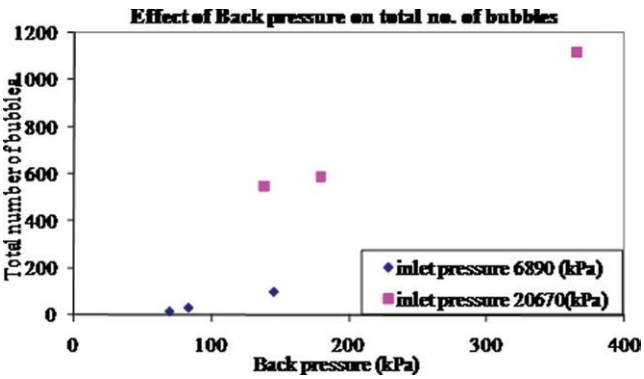

Figure 10. Effect of back pressure on total number of bubbles.

[Color figure can be viewed in the online issue, which is available at wileyonlinelibrary.com.]

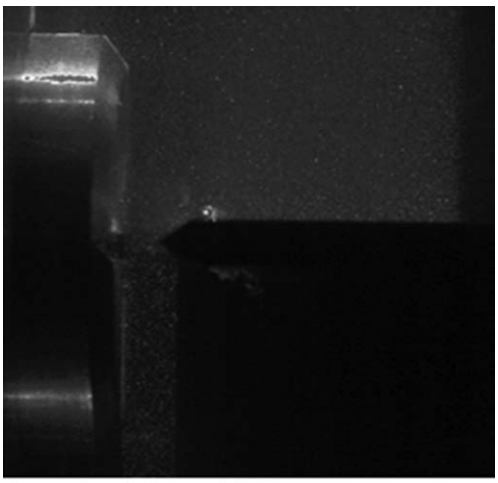

(a)

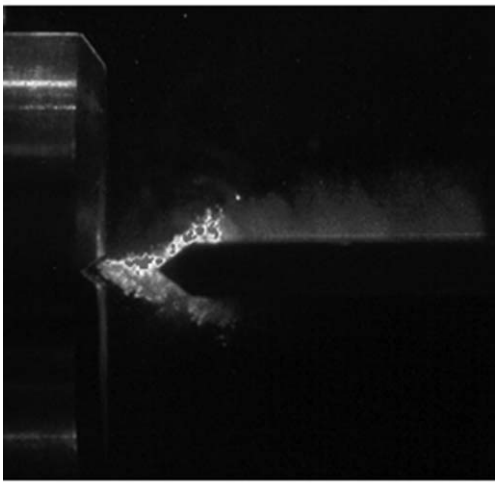

(b)

Figure 11. PIV photograph of cavitational bubble density at conditions of (a) high-back pressure and (b) low-back pressure.

size is slightly higher from 79 to 93 μm as the blade is moving from 2.2 to 8.8 mm distance away from the orifice plate, and this variation in bubble size with distance is shown in Figure 15. The presence of blade close to the orifice in effect moves the high-pressure zone close to the orifice and forces the cavitation bubbles to collapse prematurely, and hence not allowing the bubbles to grow in bigger size. The calculated total number of bubbles is decreasing from 167 to 43 as the blade moves 2.2–8.8 mm distance away from the orifice, and this variation is shown in Figure 16. The presence of blade near to the orifice causes more bubbles to form. This is because of the fragments of the prematurely, collapsed cavities become the nuclei that will experience intense vortex shedding on either side of the blade. As the jet is split and moves past the front of the blade, the nuclei should regrow and generate secondary cavitation collapsing zones on either side of the blade. This interaction is expected to reduce when the blade is moved away from the orifice. At a distance of 8.8 mm away from the orifice, the blade has no impact on cavitation. The variation of bubble size distribution with the blade position is shown in Figure 17, and this bubble size distribution is gradually shifting toward the higher bubble size range, and hence, the average size of the cavitation bubbles slightly increasing with the distance away from the orifice plate. This is also expected as the bubbles now has more time to grow to large sizes before they

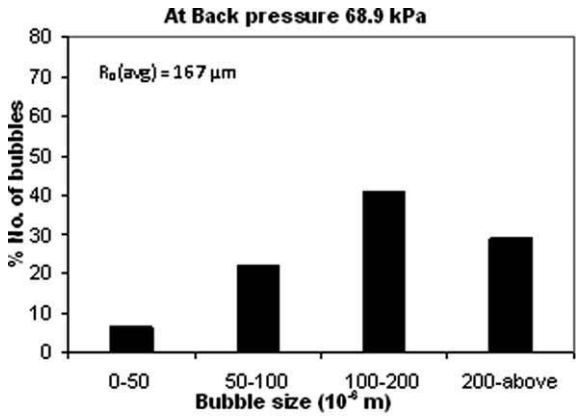

(a)

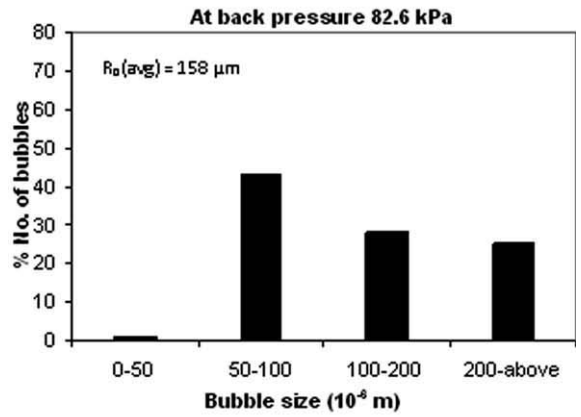

(b)

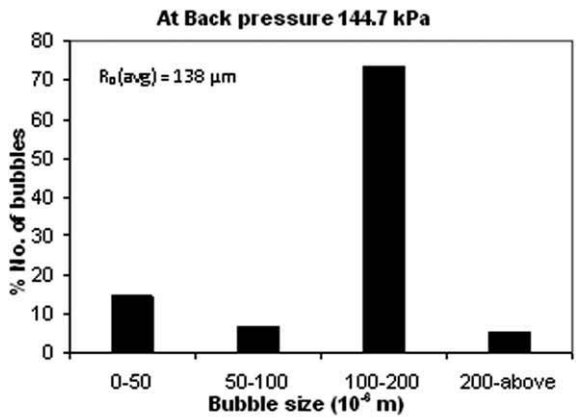

(c)

Figure 12. Effect of back pressure on cavitational bubble size distribution (6890 kPa inlet pressure).

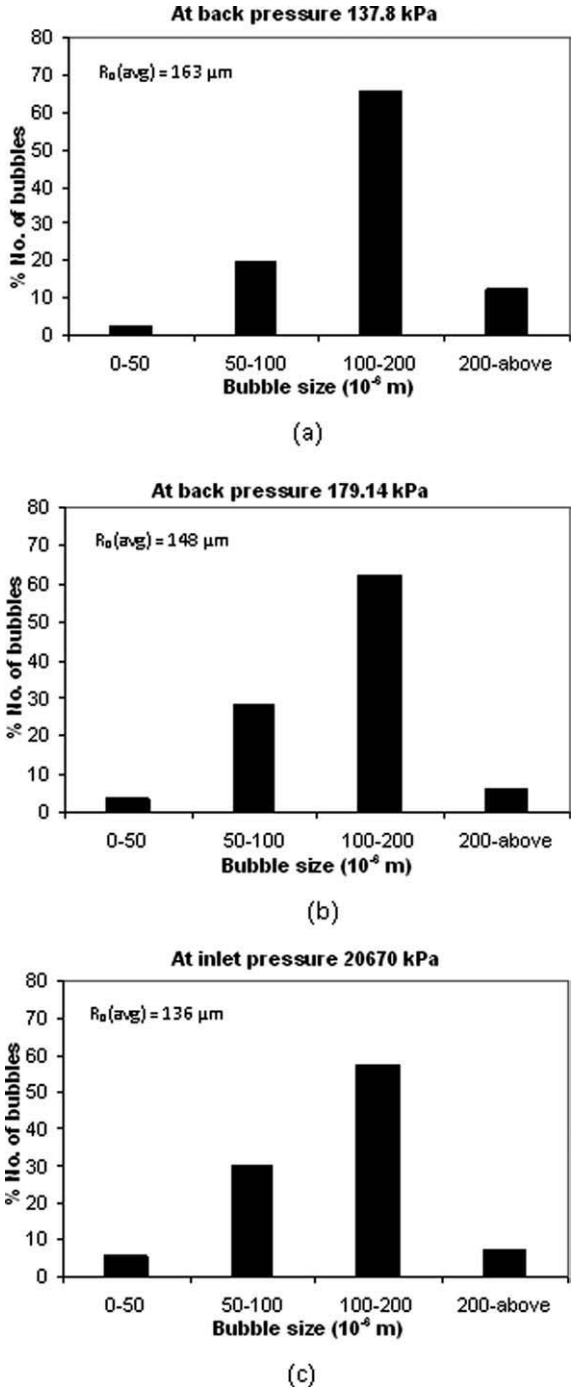

Figure 13. Effect of back pressure on cavitational bubble size distribution (20,670 kPa inlet pressure).

encounter the high-pressure zone at the leading edge of the blade.

Concluding Remarks

In this work, the effect of introducing a blade at the orifice (vena contracta) of the fast issuing jet of hydrodynamic cavitation system has been analyzed experimentally. The effect of inlet pressure, backpressure, and blade position has been analyzed within the operating conditions of the experimental system. The effect of cavitation has been quantified in the form of acoustic emission spectra (cavitation noise), bubble size, and total number of bubbles determined with a small modification to the recently developed technique of Avaaru and Pandit.[9] In this technique, shock waves radiated due to transiently collapsing bubbles have been also considered in addition to acoustic emission of stable oscillating cavitational bubbles. The effect of various parameters in hydrodynamic and resonating blade (hybrid system)

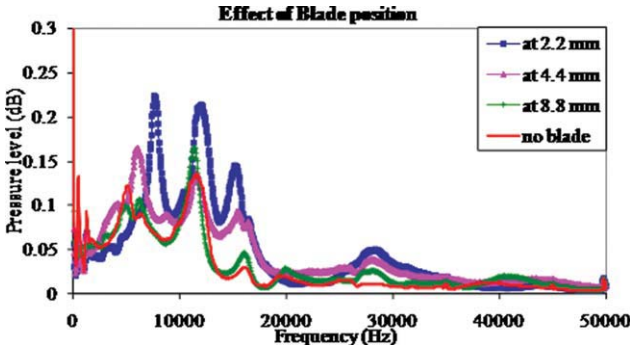

Figure 14. FFT spectrum showing the effect of blade position on the cavitation.

[Color figure can be viewed in the online issue, which is available at wileyonlinelibrary.com.]

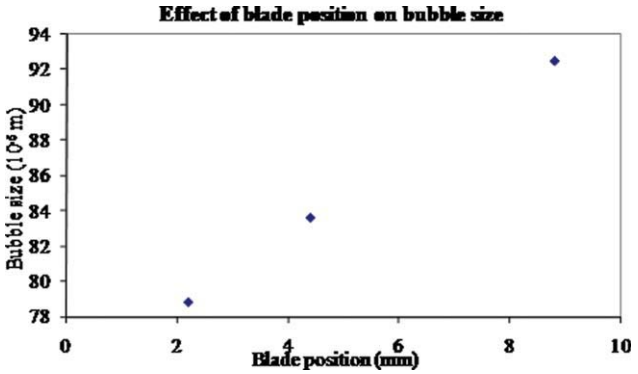

Figure 15. Effect of blade position on cavitational bubble size.

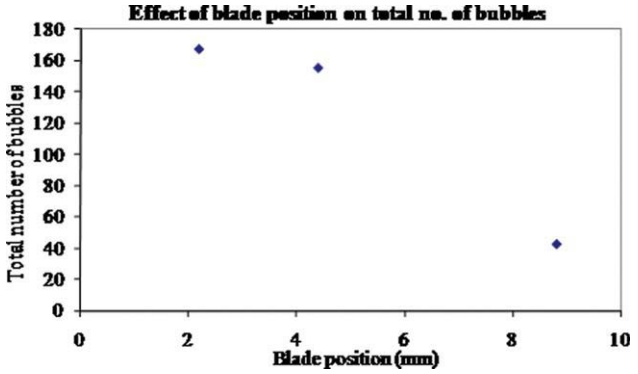

Figure 16. Effect of blade position on total number of cavitational bubbles.

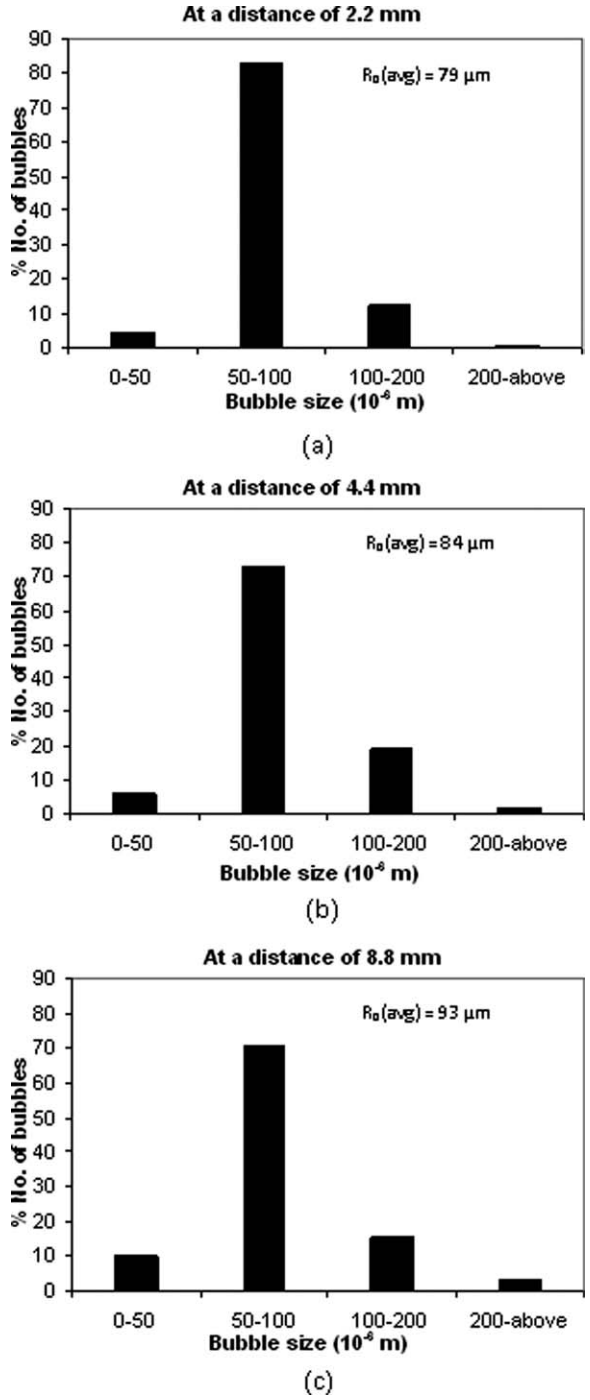

Figure 17. Effect of blade position on cavitational bubble size distribution.

cavitational system have been explained satisfactorily, based on assumption of dampening factor (0.001). The results obtained may be summarized as follows:

- The effect of inlet pressure has little impact on the bubble size, which remains in the range of 130–140 μm, but has a significant impact on the total number of bubbles (bubble density) as a result the distribution of the acoustic spectra remains the same, but the amplitude of the spectra increases at higher inlet pressures.
- At the constant inlet pressure, as the back pressure is increasing, the bubble size is decreasing; at higher back pressure, condition bubbles are unable to grow to maximum size, but the collapse intensities of each of the bubbles are very high. The total number of calculated cavitational bubbles is increasing, and hence, the increasing the net cavitational noise.
- As the blade position coming closer to the orifice, the bubble size is decreasing, i.e., bubbles are not allowed to increase in size before they are forced to collapse. As the blade position moved away from the orifice, the measured total number of bubbles are decreasing, i.e., at very close position hybrid effects of hydrodynamic and resonating blade effect is more pronounced where as at distant position hybrid effects are less pronounced.

The effect of various parameters in hydrodynamic and resonating blade (hybrid system) cavitational system have been explained satisfactorily, based on assumption of a dampening factor (0.001). A more robust method of quantifying the cavitational effects is yet to be developed, which needs a comprehensive mathematical model consists of different dampening factors for different bubbles sizes and which are at various distance from the pressure sensor (hydrophone) to explain the qualitative results obtained from the present photographic results.

For an effective scale up of hybrid hydrodynamic cavitation setup for intensification of physical processes, exact knowledge of the bubble size distribution and its concentration is of prime importance. We hope this study will contribute significantly toward the design and scale up of industrial scale hybrid hydrodynamic processors for the intensification of various physical processes.

Acknowledgments

One of the authors Dr. Ke-Ming Quan would like to acknowledge Dr. Chen Haosheng of Tsinghua University, Beijing, China, for providing the PIV photograph of cavitation bubble density shown in Figure 11.

Notation

a = length of the blade
b = width of the blade
C = wave velocity
C_V = cavitation number
E = energy delivered during cavity collapse
f_o = *f*requency of oscillation
$f_{i,j}$ = resonance frequency at mode indices (i, j)
h = Planck's constant
k_{ij} = dimensionless frequency parameter
P_b = static pressure
P_i = initial pressure
P_c = collapse pressure
P_r = pressure radiated by oscillating bubble at a distance of "r" from its center
P_{res} = resultant pressure measured by the hydrophone at a particular frequency of "f"
P_v = vapor pressure
P_∞ = ambient pressure (back pressure)
r = distance between bubble center to the hydrophone
R_o = initial radius (expanded cavity)
R_c = critical radius
V = velocity of liquid
W = average power delivered by the cavity

Greek letters

ρ = density of the liquid
λ = young's modulus
υ = passion's ratio
γ = specific heat ratio
τ = time of collapse

Literature Cited

1. Suslick KS, Mdleleni MM, Reis JT. Chemistry induced by hydrodynamic cavitation. *J Am Chem Soc*. 1997;119:9303–9304.
2. Taleyarkhan RP, West CD, Cho JS, Lahey RT Jr, Nigmatulin RI, Block RC. Evidence for nuclear emissions during acoustic cavitation. *Science*. 2002;8:1868–1873.
3. Mason TJ. Large scale sonochemical processing: aspiration and actuality. *Ultrason Sonochem.* 2000;7:145–149.
4. Dahnke S, Keil FJ. Modelling of sound fields in liquids with a non-homogenous distribution of cavitation bubbles as a basis for the design of sonochemical reactors. *Chem Eng Technol*. 1998;21:873–877.
5. Gogate PR, Pandit AB. Hydrodynamic cavitation: a state of the art review. *Rev Chem Eng*. 2001;17:1–85.
6. Mahulkar AV, Bapat PS, Pandit AB, Lewis FM. Steam bubble cavitation. *AIChE J*. 2008;54:1711–1724.
7. Senthilkumar P, Pandit AB. Modelling of hydrodynamic cavitation. *Chem Eng Technol*. 1999;22:1017–1027.
8. Arakeri VH, Chakraborty S. Studies towards potential use of ultrasonics in hydrodynamic cavitation control. *Curr Sci*. 1990;59:1326–1333.
9. Avvaru B, Pandit AB. Oscillating bubble concentration and size distribution using acoustic emission spectra. *Ultrason Sonochem*. 2009;16:105–115.
10. Minnaert M. On musical air bubbles and sound of running water. *Philos Mag*. 1993;16:235–248.
11. Pandit AB, Varley J, Thorpe RB, Davidson JF. Measurement of bubble size distribution: an acoustic technique. *Chem Eng Sci*. 1992;47:1079–1089.
12. Knapp RT. *Cavitation*. New York: McGraw-Hill, 1970.
13. Yan Y, Thorpe RB, Pandit AB. *Cavitation noise and its suppression by air in orifice flow*. In: *Symposium on Flow Induced Vibration and Noise*. Chicago, USA: ASME, 1998:25–40.
14. Blevins RD. *Formulas for Natural Frequency and Mode Shape*. New York: Van Nostrand Reinhold, 1979:492.
15. Gogate PR, Tayal RK, Pandit AB. Cavitation: a technology on the horizon. *Curr Sci*. 2006;91:35–46.

Appendix

A sample calculation for the measurement of cavity bubble size distribution and total number of bubbles have been shown in this section.

The operating conditions are 365.17 and 20,670 kPa at inlet and back pressure conditions, respectively. The measured pressure signal using hydrophone has been reconstructed at each frequency interval range of 5 kHz using inverse FFT reconstruction procedure; it is shown in the literature of Avvaru and Pandit.[9]

Table A1. FFT Reconstructed Pressure Signal, Bubble Size and Total Number of Bubbles

Frequency Range (kHz)	Reconstructed Pressure Magnitude (kPa)	Bubble Size (μm)	Total Number Bubbles
0–5	0.345	608.8	7.9
5–10	0.698	202.9	293.9
10–15	0.619	121.8	641.3
15–20	0.688	86.9	29.6
20–25	0.417	67.64	37.4
25–30	0.318	55.34	41.4
30–35	0.067	46.83	3.1
35–40	0.088	40.58	8.7
40–45	0.122	35.81	24.7
45–50	0.112	32.42	29.8

Total number of bubbles = 1117, average bubble size = 136 μm. The bubble size distribution for the same has been shown in the Figure 6c.

The magnitude of the reconstructed pressure signal in the frequency range of 15–20 kHz (average 17.5 kHz) is 0.688 kPa.

The size of the cavity measured using Minnaert's Eq. 4, $f_o = \frac{1}{2\pi}\left(\frac{3\gamma P_\infty}{\rho R_o^2}\right)^{1/2}$.

Where γ = specific heat ratio of gas contents = 1.6 and ρ = density (1000 kg/m^3).

P_∞ = operating pressure (static pressure) at the point of measurement, it is summation of vapor pressure and 4% of back pressure recovery, i.e., 19,033 Pa.

At these operating conditions, the calculated bubble size of this frequency range bubbles is 86.97 μm.

Radiated (acoustic emission) pressure due to the stable oscillation of this single bubble calculated from Eq. 5, $p_r = \frac{(3\gamma P_\infty \rho)^{1/2}}{\pi f_o r} = 17.45$ Pa.

Total number of bubbles oscillating at this oscillating frequency calculated from Eq. 6 is equal to 30 (approximately).

Similarly, all the bubbles oscillating at different vibrational frequencies at the interval range of 5 kHz have been calculated, and it is given in Table A1.

Manuscript received Oct. 27, 2010, and revision received May 5, 2010.